Synchronization for IR-UWB System Using a Switching Phase Detector-Based Impulse Phase-Locked Loop

Lin Zheng, Zhenghong Liu, and Mei Wang

Conventional synchronization algorithms for impulse radio require high-speed sampling and a precise local clock. Here, a phase-locked loop (PLL) scheme is introduced to acquire and track periodical impulses. The proposed impulse PLL (iPLL) is analyzed under an ideal Gaussian noise channel and multipath environment. The timing synchronization can be recovered directly from the locked frequency and phase. To make full use of the high harmonics of the received impulses efficiently in synchronization, the switching phase detector is applied in iPLL. It is capable of obtaining higher loop gain without a rise in timing errors. In different environments, simulations verify our analysis and show about one-tenth of the root mean square errors of conventional impulse synchronizations. The developed iPLL prototype applied in a high-speed ultra-wideband transceiver shows its feasibility, low complexity, and high precision.

Keywords: Synchronization, impulse radio, ultra-wideband communication, phase-locked loop, phase detector.

I. Introduction

Impulse radio ultra-wideband (IR-UWB) is becoming one of the candidate proposals in the physical layers of indoor multimedia and wireless sensor networks (WSNs) due to its high capacity and ranging ability [1], [2]. To reduce the complexity for implementation, receivers based on noncoherent techniques are increasingly popular in IR-UWB communications [3]. However, a noncoherent receiver requires high-precision synchronization.

Generally, synchronization in a UWB receiver depends on high-speed sampling, sophisticated signal processing, and a highly-precise delay line [4]-[6]. In recent years, samplings at the sub-Nyquist rate, or frame rate in timing recovery, have been further developed [7]-[11]. Noncoherent methods, such as differential and energy detection, are important for reducing complexity. In [8], the timing with a dirty template (TDT) algorithm applying a differential correlator is introduced to recover timing synchronization without channel information. Reversing alternate symbols produces a unique peak simultaneously with the arrival of impulses in a frame. When the delay spread of the channel is far longer than the frame duration, an uncertain deviation appears in this algorithm. Wang proposed the weighted energy detection method for timing synchronization (that is, the detection is based on weighted energy blocks) [10]. In [11], Liu proposed a process after orthogonal-codeword matching to suppress the interframe and intersymbol interference effectively. However, synchronization precision is still limited by the searching step-size and noncoherent detection, even if the synchronization

Manuscript received May 15, 2011; revised Aug. 6, 2011; accepted Aug. 24, 2011.

This work was supported by the National Natural Science Foundation (No. 60962001) of China, and Guangxi Nature Science Foundation (No. 0991018Z, No. 0731026).

Lin Zheng (phone: +86 077 3229 1274, gwzheng@gmail.com), Zhenghong Liu (cnzlin@yahoo.com.cn), and Mei Wang (mwang@guet.edu.cn) are with the Key Lab. of Cognitive Radio & Information Processing, the Ministry of Education, Guilin University of Electronic Technology, Guilin, China.

http://dx.doi.org/10.4218/etrij.12.0111.0299

only requires symbol-rate sampling, the precision of the analog delay line that is unable to be integrated in a CMOS chip, and the stability and accuracy cycle of the local oscillator consistent with the transmitter.

To further simplify the receiver, acquisition schemes in the analog front end are proposed for IR-UWB synchronization. Therefore, a receiver is not necessary to sample at a high rate. In [12], [13], the well-known delay phase-locked loop (PLL)-like theory is introduced to construct an acquisition circuit. An approach based on sampling-and-hold PLL is presented in [14], [15] to synchronize the received impulses. The proposed PLLs in the UWB receiver require a pulse waveform close to the truncated sinusoid so that coherent phase detection is achieved. This means the cycle of the voltage-controlled oscillator (VCO) should reach the width of the UWB pulse (less than a nanosecond). Secondly, in practice, it is troublesome to address a waveform distorted by dense multipath propagation.

Based on the theory drawn from sampling PLL in the frequency-multiplier synthesizer [16], [17], we introduce a synchronization scheme for impulse radio. For high-precision delay and short-acquisition delay, a nonlinear phase detector (PD), that is, a switching PD, is derived to capture higher harmonics of pulses and avoid their interferences at the same time. The analysis and simulation verify the outstanding performance of the scheme. The proposed method has been applied in the timing recovery circuit of our high-speed IR communication system. The results of this implementation are also shown at the end of the paper.

The rest of this paper is organized as follows. Section II provides the signal model and introduces the synchronization theory of impulse PLL (iPLL). Section III analyzes timing synchronization in a UWB multipath channel. Section IV presents and analyzes a switching PD for improving performance of the proposed iPLL. Simulation and implementation in practice are discussed in section V. Finally, conclusions are drawn in section VI.

II. Synchronization with iPLL

In this section, we focus on binary impulse amplitude modulation (PAM) with positive and negative levels, which can be applied in other detectors by similar principle. A square-law device is applied before the proposed iPLL, and its output is

$$u_i(t) = U_i \sum_{n=1}^{\infty} g(t - nT_1 + T_{\theta i}) + v(t), \quad (1)$$

where $g(t)$ is the output of the energy detector, T_1 is the frame cycle with one pulse per frame, $T_{\theta i}$ refers to the time delay of the first arrival channel path, and $v(t)$ is the noise item. Assume that the received noise is a zero-mean additive white Gaussian process with two-sided power spectral density (PSD) $N_0/2$ and bandwidth B. Conventional energy detectors have been analyzed by [21], and squared noise $v(t)$ obeys χ^2 distributions. Even if spread by the square-law device, the width of the impulse conforms to $T_p \ll T_1$.

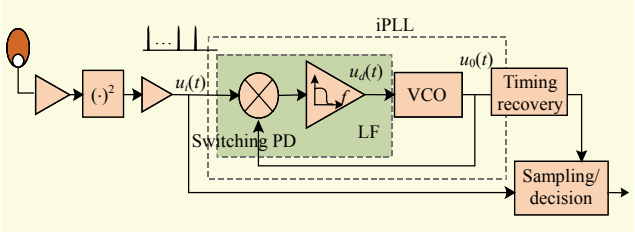

Fig. 1. PLL for IR.

The structure of the proposed PLL is shown in Fig.1. The angle frequency of the VCO is w_0, that is, close to $w_1 = 2\pi / T_1$. The multiplier is a PD, whose results are stored in the loop filter, an ideal active integrator. The timing recovery module contains a clock shaper to directly shape the continuous sinusoid to the synchronized clock.

Borrowing an idea from the theory of the sampling PLL in a frequency synthesizer [17], we can analyze the proposed UWB iPLL in a similar way. In our scheme, the received dirty impulses, which are deformed and noised in propagation, replace the ideal sampling signals in the synthesizer, and the output of local VCO is not the frequency multiplication but the recovered timing synchronization. The cycle of the oscillator in the receiver is identical to the frame rate of the received pulses. However, the performance of the proposed PLL is limited by the low energy of the base harmonic of the impulse signal.

The sinusoid of the VCO is given by

$$\begin{aligned} u_0(t) &= \sin(w_0 t + \theta_0) = \sin(w_1 t + (w_0 - w_1)t + \theta_0) \\ &= \sin(w_1 t + \theta_2(t)), \end{aligned} \quad (2)$$

where $w_1 = 2\pi / T_1$ and $\theta_2(t) = (w_0 - w_1)t + \theta_0$. The PD is implemented conventionally by a linear multiplier. Thus, the result of the phase detection and filtering is

$$\begin{aligned} u_d(t) &= K_m \int_{-\infty}^{t} u_0(\tau) u_i(\tau) d\tau \\ &= \sum_{n=0}^{\infty} K_m U_i \sin\left[w_1(nT_1 - T_{\theta i}) + \theta_2(nT_1 - T_{\theta i})\right] \\ &= \sum_{n=0}^{\infty} K_m U_i \sin\left[-\theta_i + \theta_2(nT_1 - T_{\theta i})\right], \end{aligned} \quad (3)$$

where K_m is the gain of the PD. It is the error control voltage to drive the VCO. Substituting $nT - T_{\theta i}$ with t, we obtain the near direct-current (DC) control voltage by

$$u_d(t) = K_m U_i \sin(\theta_2(t) - \theta_i) = K_d \sin\theta_e(t), \quad (4)$$

where $\theta_e(t) = \theta_2(t) - \theta_i$ and $K_d = K_m U_i$. This is a

conventional loop equation in PLL. Similar to that of the PLL in [16], we deduce the noise performance of the proposed iPLL in Appendix A. The steady-state phase variance is derived as

$$\sigma_{\theta 2}^2 = \frac{\sigma_v^2}{K_d^2} \cdot \frac{B_L}{B/2} = \sigma_{\theta 1}^2 \cdot \frac{2B_L}{B}, \quad (5)$$

where B is the bandwidth of the input signal, $\sigma_{\theta 1}^2 = \sigma_v^2 / K_d^2$ is the variance of the equivalent input phase noise, and $B_L = \int_0^{B/2} |H(j2\pi f)|^2 \, df$ is defined as the loop noise bandwidth in which $H(j2\pi f)$ is the transfer function of the loop. Generally, it obeys $B_L \ll B/2$ in conventional PLL. As presented in (5), the proposed PLL has noise-suppression capability, which is important to synchronization. Note that the timing error $\Delta T = \Delta\theta_2 / w_1$, so the timing variance is

$$E[(\Delta T)^2] = \frac{\sigma_{\theta 2}^2}{w_1^2} = \frac{\sigma_v^2}{K_d^2 w_1^2} \cdot \frac{2B_L}{B}. \quad (6)$$

III. Acquisition in Multipath Channel

In wireless UWB communications, the impulses are significantly distorted by dense-multipath propagation and non-ideal RF devices, which results in pulse dispersion and intersymbol interference. The equalizations and channel estimations must depend on complicated signal processing under this condition. Noncoherent detection is an efficient way to capture energy of these dispersive signals with low cost. Here, the energy detector extracts the envelope of the received impulses by square-law devices. Due to the negative exponential decay of the multipath profile, the waveform from the square-law device can be simplified as

$$M_i(t) = U_i \sum_{n=1}^{\infty} e^{-\mu_0 t} u(t - nT_1 + T_{\theta i}), \quad (7)$$

where μ_0 is the rate of exponential decay and $u(t)$ is the step function.

The relation between the VCO phase and peak of the received multipath impulse is dealt with below.

Without loss of generality, we can set $T_{\theta i} = 0$ and assume there is no frequency difference between the local frequency of the receiver and the frame frequency of received impulses, that is, $w_1 = 1/T$. The error control voltage from the loop filter is

$$\begin{aligned} u'_d(\theta_2) &= \int_0^{\frac{2\pi}{w_1}} K_m M_i(t) \sin(w_1 t + \theta_2) dt \\ &\approx U_i K_m \int_0^{\frac{2\pi}{w_1}} e^{-\mu_0 t} \sin(w_1 t + \theta_2) dt \\ &= \frac{U_i K_m}{\mu_0^2 + w_1^2} \left(1 - e^{-\frac{2\pi\mu_0}{w_1}}\right)\left(\mu_0 \sin\theta_2 + w_1 \cos\theta_2\right). \end{aligned} \quad (8)$$

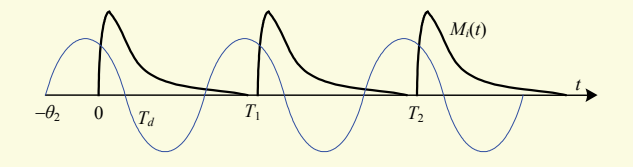

Fig. 2. Signals at steady-locked status of iPLL.

It is well known that the steady-state control voltage of PLL approaches zero when a loop is locked, that is, $u'_d(\theta_2) \approx 0$. Thus, by solving (8), we can obtain two solutions: $\theta_2 = -\arctan(w_1/\mu_0)$ and $\theta_2 = \pi - \arctan(w_1/\mu_0)$. According to PLL theory [16], the former is a saddle point and the latter is a convergent one. Figure 2 shows the phase relationship between the received impulses and the sinusoid signal of the VCO. The phase π of sinusoid corresponding to the center of gravity of the impulse can be approximated as the desired sampling tick. This tick is presented as

$$\begin{aligned} T_d &= \frac{\pi - \theta_2}{w_1} = \frac{\pi - \pi + \arctan(w_1/\mu_0)}{w_1} \\ &= \frac{1}{w_1}\arctan(w_1/\mu_0) \approx \frac{1}{\mu_0}. \end{aligned} \quad (9)$$

In line-of-sight (LOS) and non-line-of-sight (NLOS) propagation environments, we note that the decay rate μ_0 is obviously different. Under the LOS condition, the fast decay of the multipath impulse, that is, $\mu_0 \gg 1$, leads to the closeness between the peak of the received impulse and the tick of phase π. Under the NLOS condition, the slow decay of an impulse may cause phase deviation, while the difference in the amplitude of the samples can be ignored. Therefore, by shaping the sinusoid to a square wave, the synchronous clock is able to be directly recovered.

The deviation of timing synchronization from an optimum sampling point is determined by the channel parameters μ_0 and the noise variance N_0. Theoretically, the deviation could be corrected using a priori knowledge of this channel. In practice, a coarse correction estimated by the length of the multipath delay spread is enough in a certain range of wireless communication.

IV. Switching Phase Detector

In practice, the envelope out from the energy detector becomes wider than the transmitted impulses, due to multipath propagation and low-pass devices. The iPLL mentioned above is constructed on the base harmonic of the frame rate impulses. However, this base harmonic of the waveform consumes merely a small part of the impulse's power. The higher harmonics are not employed, yet still interfere with the loop.

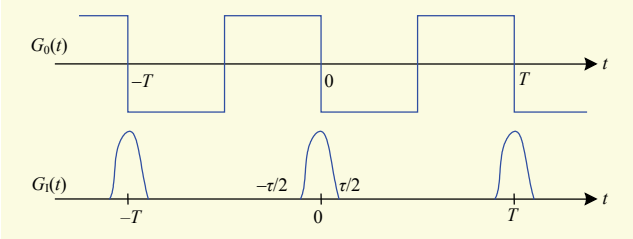

Fig. 3. Equivalent inputs to linear PD in analysis of switching phase detection.

Note that the phase of higher harmonics is identical to that of the base harmonics in a narrow pulse, so we can make use of the higher harmonics for enhancing acquisition.

For simplifying the analysis, the envelopes demodulated from the noncoherent detector are approximated as narrow rectangle pulses. Fourier expansion for the pulses is given by

$$G_1(w_1 t+\theta_i)=\frac{U_i\tau}{T_1}+U_i\sum_{n=1}^{\infty}\frac{2}{n\pi}\sin\left(\frac{n\pi\tau}{T_1}\right)\cos(nw_1 t+n\theta_i), \quad (10)$$

where τ is the multipath spread of the impulse. The conventional PLL adopts a linear multiplier as the PD for acquiring and tracking the continuous sinusoid [16]. Their principles are analyzed, and the higher harmonics of the switcher are just regarded as a source of the ripple [22]. Here, using a switching PD instead of a linear multiplier in iPLL, we obtain better performance for the UWB impulse without complicating the circuit.

As shown in Fig. 3, the squared wave $G_0(t)$ is equivalent to the switcher driven by the sinusoid output from the VCO. It is periodic and can be expanded in a Fourier series as

$$G_0(w_1 t+\theta_2(t))=\sum_{n=1}^{\infty}\frac{4}{n\pi}\sin^2\left(\frac{n\pi}{2}\right)\sin(nw_1 t+n\theta_2(t)). \quad (11)$$

The multiplier's output is the sum of each individual term of the Fourier series multiplied by the input signal. The error control signal (DC) from the loop filter is derived in Appendix B, and is given as

$$\begin{aligned} u_d'(t)&=\int_{-\infty}^{t}K_m G_0(\tau)G_1(\tau)d\tau \\ &=\sum_{n=1}^{\infty}\frac{8U_iK_m}{n^2\pi^2}\sin^2\left(\frac{n\pi}{2}\right)\sin\left(\frac{n\pi\tau}{T_1}\right)\sin(n\theta_e(t)) \\ &\approx\sum_{n=1}^{\infty}\frac{8U_iK_m}{n\pi^2}\sin^2\left(\frac{n\pi}{2}\right)\sin\left(\frac{n\pi\tau}{T_1}\right)\sin(\theta_e(t)). \end{aligned} \quad (12)$$

Clearly, the higher-order harmonics in the received pulses contribute the DC component $\sin\theta_e$. Thus, the loop gain K is multiplied by

$$k=\sum_{n=1}^{\infty}\frac{8}{n\pi^2}\sin\left(\frac{n\pi\tau}{T_1}\right), \quad n=1,3,5,... \quad (13)$$

Next, we consider the phase noise in the modified iPLL. The phase variance is comprised of noise components due to the harmonics. The equivalent input phase variance corresponding to the n-th harmonic is given by

$$\begin{aligned} \sigma_{\theta vi}^2(n)&=\sigma_v^2\left(\frac{4/n\pi}{U_i k}\right)^2 \\ &=\sigma_{\theta 1}^2\cdot\frac{16}{n^2\pi^2k^2}, \quad n=1,3,5,... \end{aligned} \quad (14)$$

The output phase variance due to the n-th harmonic of the squared wave is derived as

$$\begin{aligned} \sigma_{\theta vo}^2(n)&=\sigma_{\theta vi}^2(n)\cdot\frac{2B_L(n)}{B} \\ &=\sigma_{\theta vi}^2(n)\cdot\frac{2B_L\cdot k_n}{B}=\frac{16}{n^2\pi^2k^2}\cdot k_n\cdot\sigma_{\theta 2}^2 \\ &\approx\frac{128}{n^4\pi^4k^2}\cdot\sin\left(\frac{n\pi\tau}{T_1}\right)\cdot\sigma_{\theta 2}^2 \\ &=\frac{2\sin(n\pi\tau/T_1)}{n^4\left[\sum_{m=1}^{\infty}\frac{1}{m^2}\sin(m\pi\tau/T_1)\right]^2}\cdot\sigma_{\theta 2}^2, \\ n,m&=1,3,5,... \end{aligned} \quad (15)$$

where k_n is the loop bandwidth increment of the n-th harmonic. It approximates the multiple of the loop gain K, that is, $K(n)=k_nK$. k_n is approximated as

$$k_n\approx\frac{8}{n\pi^2}\sin\left(\frac{n\pi\tau}{T_1}\right), \quad n=1,3,5,... \quad (16)$$

Therefore, the total phase variance is $\sigma_{\theta vo}^2=\sum_{n=1}^{\infty}\sigma_{\theta vo}^2(n)$. To compare the noise performance between the switching PD and linear PD, we define η as the ratio of loop increment, that is, gain K to that of the phase noise, that is,

$$\eta=k\times\left(\sum_{n=1}^{\infty}\frac{16k_n}{n^2\pi^2k^2}\right)^{-1}=\frac{\pi^2k^3}{16\sum_{n=1}^{\infty}k_n/n}. \quad (17)$$

Figure 4 plots the ratio η when $0<\tau/T_1<1$. By comparing this with the results of the linear PD, we obtain the suppression of output phase variance when the width of the pulses is narrower, that is, $\tau\ll T_1$. Even if the duty ratio η is high, the phase-noise performance decreases slightly. It is just what we expected in low-rate radio communication.

A linear PD can be viewed as a special case of a nonlinear PD. Assigned n=1, the noise phase variance under the linear PD is deduced as

$$\sigma_{\theta vo}^2=\frac{2}{\sin(\pi\tau/T_1)}\cdot\sigma_{\theta 2}^2. \quad (18)$$

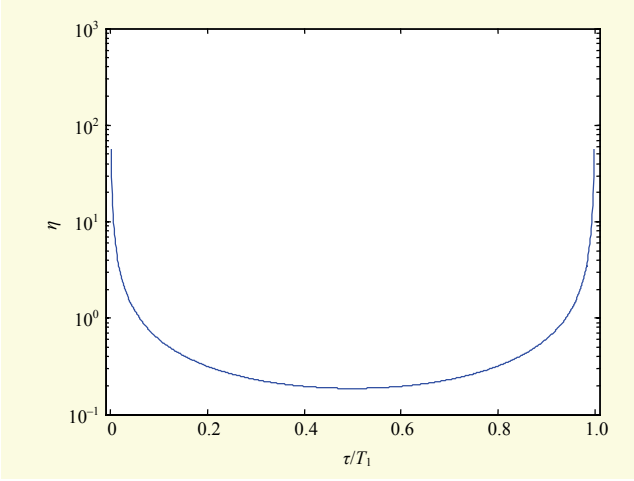

Fig. 4. Performance analysis of switching PD for impulse signals.

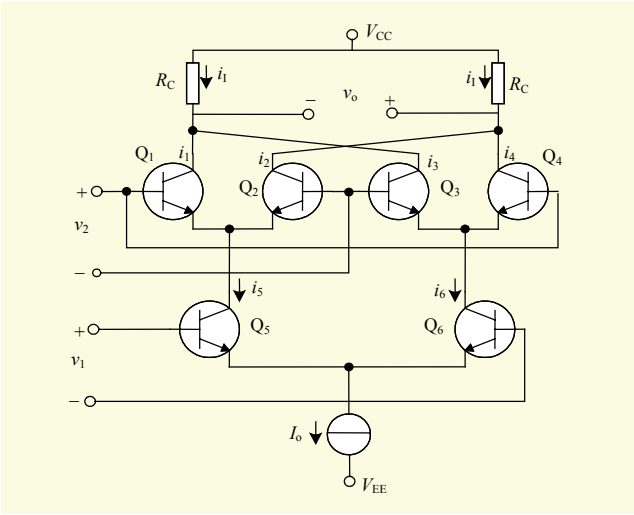

Fig. 5. Gilbert multiplier cell.

The Gilbert cell shown in Fig. 5 is a prevalent switching PD. The circuit implements a four-quadrant analog multiplier [23] whose design is based on a double-balanced active mixer architecture comprised of a differential quad (Ql, Q2, Q3, and Q4), a differential-pair driver stage (Q5 and Q6), and bias current sources (I_0). This circuit does not have a balun so that it can be more easily integrated into a monolithic circuit.

The differential current i is given by

$$i = i_{\mathrm{I}} - i_{\mathrm{II}} = I_0 \mathrm{th}\left(\frac{v_1}{2V_{\mathrm{T}}}\right)\mathrm{th}\left(\frac{v_2}{2V_{\mathrm{T}}}\right), \tag{19}$$

where V_{T} is the thermal voltage at room temperature, approximately 26 mV, and v_1 and v_2 are inputs of the PD, that is, the received pulses and the sinusoid output from the VCO, respectively.

The received signal v_1 is usually a small signal, and the VCO output v_2 is usually a big signal, that is, $v_1 < V_{\mathrm{T}}$ and $v_2 \gg V_{\mathrm{T}}$.

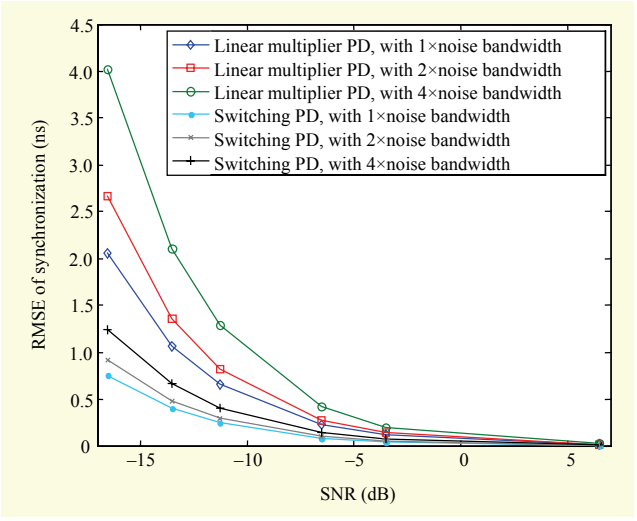

Fig. 6. RMSE of synchronization vs. SNR with different PDs and loop bandwidths. Condition: $\tau = T_1 / 20$.

Thus, (19) can be approximated as

$$i = \frac{I_0}{2V_{\mathrm{T}}} v_1 \cdot \mathrm{th}\left(\frac{v_2}{2V_{\mathrm{T}}}\right) \approx \frac{I_0}{2V_{\mathrm{T}}} v_1 G_0(v_2). \tag{20}$$

The transistors Q1, Q2, Q3, and Q4 work at the switching status, and Q1 and Q2 work in their linear area.

V. Simulations and Implementation

In this section, the performance of the proposed timing synchronization based on the iPLL and switching PD is verified by simulation. Furthermore, this scheme is implemented in a high-speed wireless UWB transceiver prototype.

The PAM signals are converted to periodic constant-amplitude impulses by the energy detector. The cycle of impulses is set to T_1=200 ns, and the local frequencies of the VCO are set to around $1/T_1$, 5.01 MHz. The active proportional plus integral filter whose bandwidth is limited to 100 kHz is adopted as the loop filter.

In Fig. 6, the root mean square errors (RMSEs) of the timing recovery using the proposed iPLL and a switching PD are depicted. In PLL theory, the loop noise bandwidth B_L is controlled by the gain of the VCO, that is, K_0 [16]. We experimented with loop noise bandwidth, multiplying once, twice, and four times, by adjusting K_0. As a result, the RMSE increases about two and four times on a bandwidth basis. This is consistent with the result given in (6). On the other hand, the figure shows that a highly-precise synchronization in a low-SNR channel is achieved by switching PD. Consistent with the analysis of (15) and the iPLL theory described in section II, we get higher precision with a lower loop noise bandwidth.

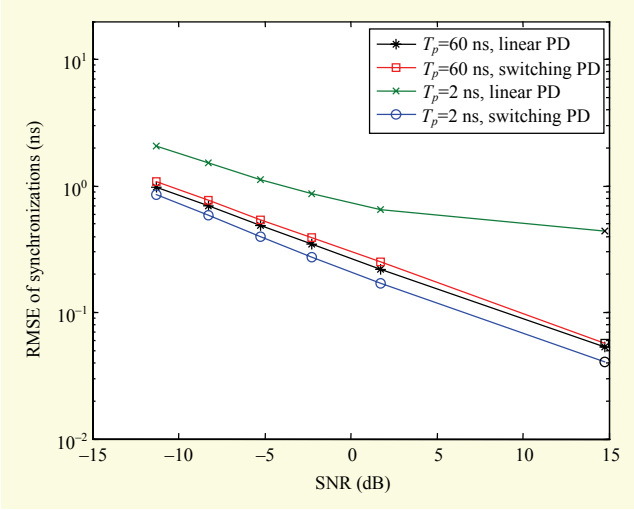

Fig. 7. RMSE of synchronization vs. SNR with different widths of injected impulses.

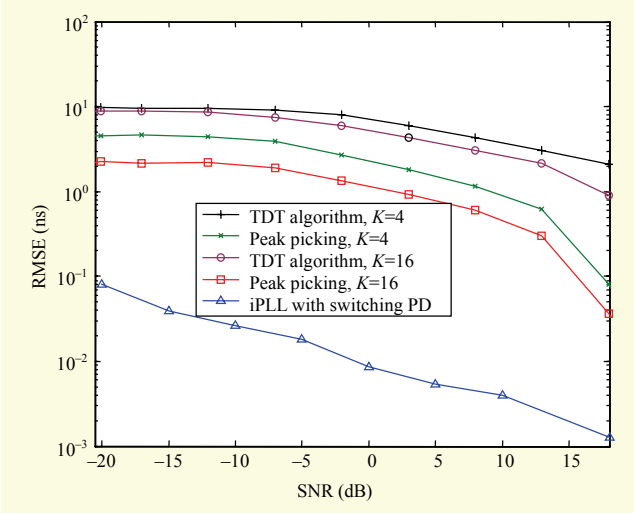

Fig. 8. Timing RMSEs between synchronization algorithms in LOS UWB environment.

Two cases with 2-ns and 60-ns impulse widths are simulated while the impulse cycle is still T_1=200 ns. The loop performance with different duty-cycle impulses is illustrated in Fig. 7. The linear PD-based iPLL presents a slightly lower RMSE compared with that based on a switching PD at a high duty cycle. On the contrary, a switching PD-based iPLL significantly outperforms a linear one. The simulations are identical to the theoretical solutions in the section IV. Therefore, the proposed switching PD is verified to be a good choice in application.

To verify the performance of the proposed iPLL, two timing algorithms are simulated and compared in a multipath channel. They are the peak-picking algorithm based on fractional-nanosecond sampling [7] and the TDT algorithm based on symbol-rate sampling [8]. The former exhaustively searches over the fractional-nanosecond-based samples for the peak of the multipath signal. The latter acquires it by differential correlation. The precision of the TDT algorithm is limited by the searching step-size even though it only requires symbol-rate sampling. In our simulations, K samples in the above two algorithms are cumulated to average out the additive noise effects.

Wideband channel models for spread-spectrum systems are evaluated to be effective [18], [19]. In addition, there are some new characteristics in the UWB multipath channel [1], such as a dense multipath. Here, LOS and NLOS UWB multipath channels are generated using the first and second channel models (CM1 and CM2) in IEEE802.15.3a standard [20]. CM1 describes an LOS scenario with a separation between the transmitter and receiver of less than 4 m. CM2 describes the same range but for an NLOS situation. In this experiment, the width of the transmitted pulse is 2 ns, and the impulse rate is $1/T_1$=20 MHz. To guarantee acquisition speed, the bandwidth of the loop filter in iPLL is160 kH. To meet the requirement of the TDT algorithm, the alternate-symbol PAM impulse is set to the reverse of each other.

Simulation results plotted in Figs. 8 and 9 are the RMSE of timing synchronization. In the LOS environment, the transient peak of impulses is highly related to the noise. We call it high-transient SNR. The effect of energy detection approaches that of a coherent method. Therefore, the peak-picking method obtains a lower RMSE than the TDT algorithm over all SNR conditions. The proposed iPLL with a switching PD outperforms the two synchronizers. Even in low SNR conditions, the precision of acquisition is up to the degree of 0.1 ns. The result also verifies the outstanding performance achieved by the switching PD in the case of a low duty-cycle.

In an NLOS environment, the transient peaks of the impulses reduce and delay the spread increase. The performance degradation of the peak-picking method is comprehensible. The differential correlation-based TDT algorithm captures most of the scattered energy of the impulses. It demonstrates a better performance than that of the peak-picking acquisition at a high SNR shown in Fig. 9. Even by a multipath delay spread, the iPLL presents the lowest RMSE of the three methods. This is mainly a result of the strong interference resistance of PLL.

When the multipath delay spread further increases, the envelope is distorted and unable to be viewed as a negative exponential curve. In this case, it must be pointed out that the tick T_d in section III may be at the trough of the envelope signal of the square-law device. The sampling clock extracted from this locked loop may deviate from the optimal peak point of the detecting signal.

The proposed iPLL is implemented in the 100-Mbps OOK-

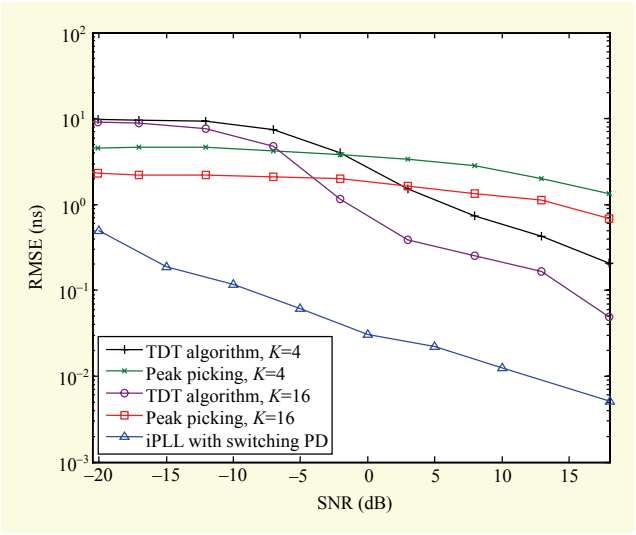

Fig. 9. Timing RMSEs between synchronization algorithms in NLOS UWB environment.

Fig. 10. Acquisition process with synchronization sequences.

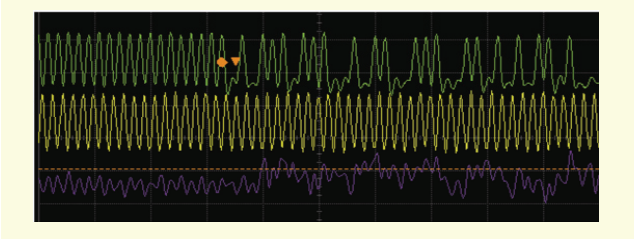

Fig. 11. Tracking modulated impulses by iPLL.

modulation transceiver prototype system. The impulse cycle is T_1=10 ns, and the width of the demodulated pulse is about $\tau = 4$ ns. A synchronization sequence is adopted before the modulated impulses. In Fig. 10, the acquisition process by iPLL is shown in a snapshot by a high-speed oscillograph. The green, yellow, and purple curves are the received impulses, local synchronized clock, and the output of the loop filter, respectively. There is a small frequency difference between the local oscillator and received frame-rate of impulses. Shown as the purple curve, through about ten impulse frame cycles, the local frequency and phase have been synchronized by the received UWB impulses. The results also indicate that there is no need to equip a high-stability and high-accuracy oscillator in an IR-UWB transceiver using an iPLL synchronizer. The tracking capability of iPLL is also measured in Fig. 11. The dithering of timing synchronization is limited in accepted bound by the narrow loop bandwidth.

VI. Conclusion

An iPLL with a switching phase detector was introduced for precise timing recovery in an impulse receiver. Interference and noise suppression by the proposed iPLL is analyzed and verified. It was also proven to be practical in a multipath UWB channel when the channel response was able to be viewed as a negative exponential descent. Furthermore, the mean square error of the switching phase detector for impulse signals was deduced. The duty cycle is discussed in performance evaluation. Simulation, theoretic results, and implementation in the UWB transceiver indicate that the iPLL with a switching phase detector achieves high-precision synchronization with low complexity.

Appendix I. Performance of iPLL

Referring to [21], the mean and variance of $v(t)$ is

$$u_v = T_1 B N_0 \sigma_v^2 = T_1 B N_0^2 + 2E_b N_0 . \quad \text{(I1)}$$

If a hold circuit in the ideal integrator is adopted by the filter as shown in Fig. 1, we can obtain the closed-loop phase equations in the Laplace domain:

$$E(s) = K_d \left[\theta_1(s) - E(s)Q(s)K_0 / s)\right], \quad \text{(I2)}$$

$$\theta_2(s) = E(s)Q(s)K_0 / s, \quad \text{(I3)}$$

where $\theta_1(s)$ is the phase of the input pulses, K_0/s is the transfer function of the VCO, $E(s)$ is the output from PD, and $Q(s)$ is the function of the loop filter. In the proposed PLL shown in Fig. 1, an ideal integrator with a transfer function of $Q(s) = 1/s$ is adopted to acquire the frequency and phase. Derived from the loop equations, the transfer function of the PLL is obtained by

$$H(s) = \frac{\theta_2(s)}{\theta_1(s)} = \frac{K_d K_0}{s^2 + K_d K_0}. \quad \text{(I4)}$$

According to [16], the equivalent input noise $V(t) = K_d v(t) \sin\theta_2(t) / U_i$ with band-width $B/2$ and variance $\sigma_V^2 = K_d^2 \sigma_v^2 / U_i^2$. The loop equations for noise are given by

$$\theta_e(s) = -\theta_2(s), \tag{I5}$$

$$[V(s) + K_d\theta_e(s)]Q(s)K_0 / s = \theta_2(s). \tag{I6}$$

Thus, the $\theta_2(s)$ responding to the noise input is derived as

$$\theta_2(s) = \frac{K_0 Q(s)V(s)}{s + K_d K_0 Q(s)} = H(s)\cdot\frac{V(s)}{K_d}. \tag{I7}$$

Note that $V(t)$ has a nearly flat power PSD in band $B/2$, and we obtain the variance of the phase $\theta_2(t)$ due to noise as

$$\begin{aligned}\sigma_{\theta 2}^2 &= \int_0^{B/2} |H(j2\pi f)|^2 \frac{2\sigma_V^2}{K_d^2 B} df \\ &= \frac{2T_1 BN_0^2 + 4E_b N_0}{U_i^2 B}\int_0^{B/2} |H(j2\pi f)|^2 \, df.\end{aligned} \tag{I8}$$

Appendix II. Output of PD

The output of the PD is derived by

$$\begin{aligned}u_d(t) &= K_m G_1(t)G_0(t) \\ &= K_m\left[\frac{U_i\tau}{T_1} + U_i\sum_{n=1}^{\infty}\frac{2}{n\pi}\sin\left(\frac{n\pi\tau}{T_1}\right)\cos(nw_1 t + n\theta_i) + n(t)\right] \\ &\times\left[\sum_{m=1}^{\infty}\frac{4}{m\pi}\sin^2\left(\frac{m\pi}{2}\right)\sin(mw_1 t + n\theta_2(t))\right] \\ &= \frac{K_m}{2}\Big[\sum_{n=1}^{\infty}\frac{8U_i}{n^2\pi^2}\sin\Big(\frac{n\pi\tau}{T_1}\Big)\sin^2\Big(\frac{n\pi}{2}\Big)\sin(n\theta_e) \\ &+ \sum_{n=1}^{\infty}\frac{4}{n\pi}\sin^2\Big(\frac{n\pi}{2}\Big)(n_c\cos n\theta_2 + n_s\sin n\theta_2) \\ &+ \frac{2\tau}{T_1}\sum_{n=1}^{\infty}\frac{4}{n\pi}\sin^2\Big(\frac{n\pi}{2}\Big)\sin(nw_1 t + n\theta_2) \\ &+ 2\Big(\sum_{n=1}^{\infty}\frac{2}{n\pi}\sin\left(\frac{n\pi\tau}{T_1}\right)\cos(nw_1 t + n\theta_i)\Big) \\ &\times[\sum_{m=1}^{\infty}\frac{4}{m\pi}\sin^2\left(\frac{m\pi}{2}\right)\sin(mw_1 t + n\theta_2(t))]_{n\neq m}.\end{aligned}$$

Except for the first one, items in $u_d(t)$ are zero-mean. By the narrow-band loop filter, the control voltage is just the items of $\sin n\theta_e$.

Acknowledgments

The authors would like to thank the reviewers for their thorough reviews and helpful suggestions.

References

[1] M.Z. Win and R.A. Scholtz, "Characterization of Ultra-wide Bandwidth Wireless Communications Channels: A Communication Theoretic View," *IEEE J. Sel. Areas Commun.*, vol. 20, no. 12, Dec. 2002, pp. 1613-1627.

[2] D. Dardari et al., "Ranging with Ultrawide Bandwidth Signals in Multipath Environments," *Proc. IEEE*, vol. 97, no. 2, 2009, pp. 404-426.

[3] K. Witrisal et al., "Noncoherent Ultra-wideband Systems," *IEEE Signal Process. Mag.*, vol. 26, no. 4, July 2009, pp. 48-66.

[4] R. Miri, Zhou Lei, and P. Heydari, "Timing Synchronization in Impulse-radio UWB: Trends and Challenges," *Proc. Joint 6th Int. IEEE Northeast Workshop Circuits Syst. TAISA Conf.*, June 2008, pp. 221-224.

[5] H.-C. Hsu and J.-H. Wen, "Timing Synchronization in Ultra-wideband Systems with Delay Line Combination Receivers," *IEEE Commun. Lett.*, vol. 11, no. 3, Mar. 2007, pp. 264-266.

[6] G. Ranjit and K. Peter, *Ultra Wideband: Circuits, Transceivers, and Systems*, Springer Science and Business Media, LLC, US, 2008.

[7] Z. Tian and G.B. Giannakis, "A GLRT Approach to Data-Aided Timing Acquisition in UWB Radios-Part I: Algorithms," *IEEE Trans. Wireless Commun.*, vol. 4, no. 6, Nov. 2005, pp. 2956-2967.

[8] L. Yang and G.B. Giannakis, "Timing Ultra-wideband Signals With Dirty Templates," *IEEE Trans. Commun.*, vol. 53, no. 11, Nov. 2005, pp. 1952-1963.

[9] S.H. Wu and N.T. Zhang, "A Two-Step TOA Estimation Method for UWB Based Wireless Sensor Networks," *J. Software*, vol. 18, May 2007, pp. 1164-1172 (in Chinese).

[10] F. Wang, Z. Tian, and B.M. Sadler, "Weighted Energy Detection for Noncoherent Ultra-wideband Receiver Design," *IEEE Trans. Wireless Commun.*, vol. 10, no. 2, Feb. 2011, pp. 710-720.

[11] B. Liu, T. Lv, and H. Gao, "Blind Synchronization and Demodulation for Noncoherent Ultra-Wideband System with Robustness against ISI and IFI," *Proc. ICC*, May 2010, pp. 1-5.

[12] A.A. DAmico, U. Mengali, and L. Taponecco, "Synchronization for DTR Ultra-wideband Receivers," *Proc. ICC*, vol. 11, June 2006, pp. 5069-5073.

[13] M. Di Renzo, F. Graziosi, and F. Santucci, "A Modified Delay Locked Loop Synchronizer for Ranging-Based Fine Timing Acquisition of Differential Transmitted Reference UWB Receivers," *Proc. 4th European Wireless Conf.*, June 2008, pp. 1-6.

[14] S. Lee, *Design and Analysis of Ultra-wideband Impulse Radio Receiver*, PhD Dissertation, University of Southern California, LA, CA, 2002, pp. 28-37.

[15] H. Huang et al., "The Structure and Performance on an Orthogonal Sinusoidal Correlation Receiver of Impulse Radio," *Proc. VTC*, Sept. 2004, vol. 2, pp. 26-29.

[16] F.M. Gardner, *Phase-Locked Techniques*, 3rd ed., John Wiley & Sons, Inc., 2005.

[17] J. Zheng, *Principle and Application of Phase-Locked Loop*, 2nd ed., People's Posts and Telecommunications Press, 1984 (in Chinese).
[18] J. Wang and L.B. Milstein, "CDMA Overlay Situations for Microcellular Mobile Communications," *IEEE Trans. Commun.*, vol. COM-43, Feb. 1995, pp. 603-614.
[19] J. Wang, and J. Chen, "Performance of Wideband CDMA with Complex Spreading and Imperfect Channel Estimation," *IEEE J. Sel. Areas Commun.*, vol. 19, no. 1, Jan. 2001, pp. 152-163.
[20] J. Foerster, *Channel Modeling Sub-committee Report Final*, IEEE P802.15 Working Group for Wireless Personal Area Networks (WPANs), 2003. http://grouper. ieee.org/groups/802/15/pub/2002/Nov02/02490r0P802-15_SG3a-Channel-Modeling-Subcommittee-Report-Final.zip
[21] F.F. Digham, M.S. Alouini, and M.K. Simon, "On the Energy Detection of Unknown Signals over Fading Channels," *Proc. ICC03*, Apr. 2003, pp. 3575-3579.
[22] J.L. Stensby, *Phase-Locked Loops*, New York: CRC Press, 1997.
[23] B. Gilbert, "A Precise Four-Quadrant Multiplier with Sub-nanosecond Response," *IEEE J. Solid State Circuits*, vol. SC-3, no. 6, Dec. 1968, pp. 365-373.

Lin Zheng received his BS and MS in communication engineering from Guilin University of Electronic Technology, Guilin, China, in 1995 and 2000, respectively, and his PhD in communication and information system from Xidian University, China, in 2007. From 2000 to 2003, he worked as a senior engineer in ZTE Corp., Shenzhen, for 3G base-station development. Since 2008, he has been an associate professor with the School of Information and Communications, Guilin University of Electronic Technology. His research interests are distributed synchronization theory, ultra-wideband communication and localization, and adaptive signal processing.

Zhenghong Liu received his BS and MS in communication engineering from Guilin University of Electronic Technology, Guilin, China, in 2004 and 2009, respectively. Now, he works as a researcher in the Key Lab. of Cognitive Radio & Information Processing, the Ministry of Education, Guilin University of Electronic Technology. His research interests are in communication circuits, ultra-wideband communications, and wireless communication.

Mei Wang received her BS and MS in communication engineering, and her PhD in electronic engineering from Xidian University, Xi'an, China, in 1984, 1989, and 2003, respectively. Currently, she is a professor of communications at Guilin University of Electronic Technology, Guilin, China. Her research interests include wireless sensor networks, ultra-wideband localization, and chaotic communications.